Structures and Properties of New Ordered Defect Phases in the Vanadium Chromium Sulfide System

P. Vaqueiro and A. V. Powell*

Department of Chemistry, Heriot-Watt University, Riccarton, Edinburgh EH14 4AS, United Kingdom

Received March 28, 2000

The system V_xCrS_2 ($0 < x \leq 1$) has been investigated by X-ray and neutron powder diffraction. Five single-phase regions have been identified. All single-phase materials adopt pseudolayered structures, in which octahedral sites between alternate pairs of close packed sulfide layers are fully and partially occupied by cations. With increasing vanadium content, rhombohedral M_2S_3, trigonal M_2S_3, monoclinic M_3S_4, trigonal 3C-M_7S_8, and hexagonal $M_{1-x}S$ structures are successively observed. All single-phase materials exhibit semiconducting behavior, consistent with a variable range hopping conduction mechanism. Magnetic properties show considerably greater variation. The phase with the lowest vanadium content (rhombohedral M_2S_3) exhibits ferrimagnetic ordering at 100(10) K. Phases with higher vanadium content also exhibit long-range magnetic ordering, with the exception of the monoclinic M_3S_4, which is a spin glass ($T_g = 40(5)$ K).

Introduction

Many transition metal dichalcogenides MX_2 adopt the CdI_2 structure, in which cations (M) occupy all of the octahedral sites between alternate pairs of hexagonally close-packed anion (X) layers, corresponding to a stacking sequence XMXXMXXMX. The structure consists of layers of edge-shared MX_6 octahedra, of overall stoichiometry MX_2, separated by a van der Waals gap in which there is a network of vacant octahedral sites. In the closely related NiAs structure, these octahedral sites are fully occupied and the stacking sequence may be represented as XMXMXMXMX. If, however, occupation of the octahedral sites in the van der Waals gap is incomplete, the vacancies may order, giving rise to a range of two-dimensional superstructures,[1−3] corresponding to stoichiometries between the extremes of MX_2 and MX. Many binary metal sulfides adopt ordered defect structures of this type,[4,5] the stoichiometry of which can be represented by the general formula M_xMS_2 ($0 < x < 1$). The two-dimensional supercells within the partially filled layers, for a variety of rational values of x are shown in Figure 1. The nature of the vacancy ordering is dependent on the defect concentration, and a particular ordering scheme may be stable over a range of compositions, which might not necessarily include the ideal composition.

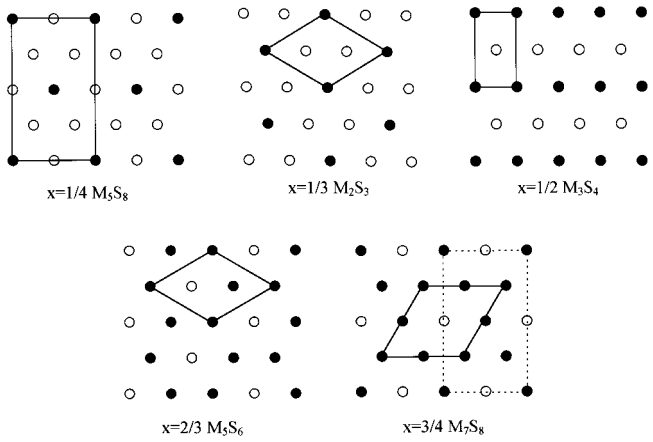

Figure 1. Arrangements of the metal vacancies within the partially occupied layers (*ab* plane) for several values of x. Black circles represent cations, white circles represent vacancies and the lines show the unit cells. For $x = 3/4$, two different stacking sequences, resulting in different unit cells, are possible. The solid line shows the unit cell of 3C-M_7S_8, while the dashed line shows that of 4C-M_7S_8.

In the Cr_xCrS_2 system, the majority of phases show a strict alternation of filled and partially filled layers, with long-range ordering within the partially filled layer. This results, with increasing x, in the successive stabilization of the rhombohedral M_2S_3, the trigonal M_2S_3, the M_3S_4, and the M_5S_6 structure types,[6] each of which is stable over only a fairly narrow range of composition. At the higher chromium content, Cr_7S_8, two different structures have been reported. While Jellinek described a NiAs-type structure,[6] with randomly distributed vacancies on the metal lattice, Popma and van Bruggen[7] reported that a sample of similar

* To whom correspondence should be addressed. Fax: +44 (0)131 451 3180. E-mail: A.V.Powell@hw.ac.uk.

(1) Tilley, R. J. D. *Crystallography and Crystal Chemistry of Materials with Layered Structures*; Lévy, F., Ed.; Reidel: Dordrecht, 1979; pp 127−184.
(2) Vaughan, D. J.; Craig, J. R. *Mineral Chemistry of Metal Sulfides*; Cambridge University Press: Cambridge, 1978.
(3) Kjeshus, A.; Pearson, W. B. *Prog. Solid State Chem.* **1964**, *1*, 83.
(4) Wold, A.; Dwight, K. *Solid State Chemistry: Synthesis, Structure and Properties of Selected Oxides and Sulfides*; Chapman and Hall: New York, 1993; ch.11.
(5) Rao, C. N. R.; Pisharody, K. P. R. *Prog. Solid State Chem.* **1979**, *10*, 207.
(6) Jellinek, F. *Acta Crystallogr.* **1957**, *10*, 620.

10.1021/cm000265c CCC: $19.00
Published on Web 08/31/2000

composition, annealed at 250 °C, adopts an ordered defect structure. All of the materials in the Cr_xCrS_2 series exhibit long-range magnetic order at low temperatures,[7−11] while the electrical properties show a gradual change from semiconducting Cr_2S_3[8] to metallic Cr_3S_4,[12] Cr_5S_6,[13] and Cr_7S_8.[14] By contrast, in the V_xVS_2 system, no well-characterized material with the M_2S_3 structure has been reported, whereas the M_3S_4 and M_5S_8 structures are stable over extended ranges of composition.[15] An ordered defect structure has also been reported for a material with a stoichiometry close to V_7S_8.[16] Both V_3S_4 and V_5S_8 are metallic antiferromagnets which exhibit temperature-independent paramagnetism above their ordering temperatures.[17,18]

The only ternary vanadium chromium sulfides reported to date are those of the M_3S_4 structure type ($x = {}^1/_2$), of general formula $V_yCr_{3-y}S_4$ ($0 < y < 3$).[19] Powder diffraction studies[20] on materials in the range $0 < y < 1$, reveal that at a critical composition of $y_c \approx 0.4$, there is an abrupt change in the distribution of vanadium and chromium cations between sites in the fully and partially occupied layers. Above y_c there is an almost statistical distribution of vanadium between both types of site, whereas at lower vanadium contents, vanadium cations preferentially occupy sites in the vacancy layer. The redistribution of cations is accompanied by changes in the magnetic and transport properties;[21] the latter involving a semiconductor to metal transition. Here, we report an extension of these investigations to ternary materials with alternative defect ordering schemes. Preparation of the series V_xCrS_2 ($0 < x \leq 1$), provides an opportunity to study changes in the structural and physical properties as both the vacancy concentration and the V/Cr ratio are varied.

Experimental Section

Mixtures of vanadium (Aldrich, 99.5%) chromium (Aldrich, 99%) and sulfur (Aldrich, 99.9%) powders, corresponding to stoichiometries V_xCrS_2 with $0 < x \leq 1$, were ground in an agate mortar and sealed in evacuated silica tubes. Prior to use, vanadium was washed with dilute HCl to remove a green oxide coating. Sealed tubes were heated initially at 500 °C for 24 h and then at 800 °C for 2 days. After regrinding under dry nitrogen, mixtures were refired in sealed tubes at 850 °C for 4 days. To homogenize the products, a regrinding and a final firing at 850 °C for 2 days was applied. Products were finally cooled to 300 °C at ∼2 °C min^{-1}, prior to removal from the furnace. However, mixtures corresponding to the compositions $x = 0.38$ and $x > 0.80$ were cooled from 850 °C to room temperature over a 24 h period. For vanadium contents with $x \geq 0.90$, some reaction of the metals with the walls of the silica tube was observed during the first firing.

Table 1. Composition Ranges of Phases in the V_xCrS_2 Series Identified by Powder X-ray Diffraction[a]

x in V_xCrS_2	observed phases
$0.13 \leq x \leq 0.30$	rhombohedral M_2S_3 + S
$0.30 < x \leq 0.35$	rhombohedral M_2S_3
0.38	complex mixture of M_2S_3 type phases
$0.40 \leq x \leq 0.46$	trigonal M_2S_3
$0.46 < x < 0.53$	trigonal M_2S_3 + M_3S_4
$0.53 \leq x \leq 0.76$	M_3S_4
$0.76 < x < 0.90$	3C-M_7S_8
$0.90 \leq x < 0.93$	$M_{1-z}S$
$0.93 \leq x \leq 1.0$	$M_{1-z}S$ + Cr

[a] All values of x refer to the stoichiometry of the initial reaction mixture.

A Philips PA2000 diffractometer with nickel-filtered Cu Kα radiation ($\lambda = 1.5418$ Å) was used for the collection of powder X-ray diffraction data. Data were collected using a step size of $2\theta = 0.02°$ and a counting time of 5 s step^{-1} over the angular range $10 \leq 2\theta/° \leq 100$. Time-of-flight powder neutron diffraction data were collected at room temperature on the Polaris diffractometer at ISIS, Rutherford Appleton Laboratory. Samples were contained in vanadium cans. Initial data manipulation and reduction was carried out using Genie[22] spectrum manipulation software. Neutron diffraction data, from the highest resolution backscattering bank of detectors ($2\theta = 145°$), were summed and normalized for subsequent use in conjunction with X-ray data in Rietveld refinement using the GSAS package.[23]

The electrical resistance of the samples as a function of temperature was measured using the 4-probe dc technique. An ingot (∼6 × 3 × 1 mm) was cut from a sintered pellet, four 50 μm silver wires were attached using colloidal silver paint and connections were made to a HP34401A multimeter. The sample was mounted in an Oxford Instruments CF1200 cryostat connected to an ITC502 temperature controller. Measurements were carried out over the temperature range $77 \leq T/K \leq 300$. Magnetic measurements were performed using a Quantum Design MPMS2 SQUID susceptometer. Samples were loaded into gelatin capsules at room temperature and data were collected over the temperature range $5 \leq T/K \leq 300$, both after cooling in zero applied field (zfc) and in the measuring field of 1000 G. Data were corrected for the diamagnetism of the gelatin capsule.

Results

Five single-phase regions and four composition regions in which there is a mixture of phases were identified by powder X-ray diffraction. The observed phases and their homogeneity regions are presented in Table 1. All values of x refer to the composition of the initial reaction mixture. Despite the precautions taken to avoid the formation of vanadium oxides, all prepared materials contain trace amounts of V_2O_3 (<1%). For reaction products with $x \approx 0.38$, powder X-ray diffraction patterns could not be indexed on the basis of any known NiAs-related superstructure. A preliminary transmission electron microscopy study[24] suggests that the

(7) Popma, T. J. A.; van Bruggen, C. F. *J. Inorg. Nucl. Chem.* **1969**, *31*, 73.
(8) Van Laar, B. *Phys. Lett.* **1967**, *25A*, 27.
(9) Van Bruggen, C. F.; Vellinga, M. B.; Haas, C. *J. Solid State Chem.* **1970**, *2*, 303.
(10) Bertaut, E. F.; Roult, G.; Aleonard, R.; Pauthenet, R.; Chevreton, M.; Jansen, R. *J. Phys.* **1964**, *25*, 582.
(11) van Laar, B. *Phys. Rev.* **1967**, *156*, 654.
(12) Holt, S. L.; Bouchard, R. J.; Wold, A. *J. Phys. Chem. Solids* **1966**, *27*, 755.
(13) Kamigaichi, T.; Masumoto, K.; Hihara, T. *J. Phys. Soc. Jpn.* **1960**, *15*, 1355.
(14) Van Bruggen, C. F.; Jellinek, F. *Propr. Thermodyn. Phys. Struct. Dériv. Semi-Métal*; CNRS: Paris, 1967.
(15) Oka, Y.; Kosuge, K.; Kachi, S. *J. Solid State Chem.* **1978**, *23*, 11.
(16) Brunie, S.; Chevreton, M.; Kauffmann, J. M. *Mater. Res. Bull.* **1972**, *7*, 253.
(17) De Vries, A. B.; Haas, C. *J. Phys. Chem. Solids* **1973**, *34*, 651.
(18) Kitaoka, Y.; Yasouka, H. *J. Phys. Soc. Jpn.* **1980**, *48*, 1949.
(19) Tazuke, Y. *J. Phys. Soc. Jpn.* **1981**, *50*, 413.
(20) Colgan, D. C.; Powell, A. V. *J. Mater. Chem.* **1996**, *6*, 1579.
(21) Powell, A. V.; Oestreich, S. *J. Mater. Chem.* **1996**, *6*, 807.
(22) David, W. I. F.; Johnson, M. W.; Knowles, K. J.; Moreton-Smith, C. M.; Crisbie, G. D.; Campbell, E. P.; Graham, S. P.; Lyall, J. S. Rutherford Appleton Laboratory Report, RAL-86-102, 1986.
(23) Larson, A. C.; von Dreele, R. B. *General Structure Analysis System*; Los Alamos Laboratory: Los Alamos, NM, 1994; Report LAUR 85-748.
(24) Crosnier-Lopez, M. P.; Vaqueiro, P. Unpublished results.

products consist of a complex mixture of phases with compositions close to $x = 0.38$.

Detailed structural studies of materials in each of the single-phase regions were performed using Rietveld analysis of powder X-ray and neutron diffraction data and are described below. The use of data from both techniques simultaneously, allows the distribution of vanadium and chromium cations between sites in the vacancy and fully occupied layers to be established. In all refinements, the neutron data background was described by a power series in $Q^{2n}/n!$, whereas that in the X-ray data was modeled using a power series in $n!/Q^{2n}$. The peak shape in the X-ray data was described by a pseudo-Voigt function and that of the neutron data by a convolution of an exponential and a pseudo-Voigt function. The peak shape coefficients were included as refinable parameters. For compositions with a vanadium content $x > 0.5$, a region centered at $d \approx 2.2$ Å was excluded from the neutron data, owing to the presence of features due to instrumental vanadium ($d = 2.141$ Å) and the (113) reflection of V_2O_3 ($d_{113} = 2.186$ Å).[25]

Composition Range $0.30 < x \leq 0.35$. Over this composition range the product appears to be a single phase of the rhombohedral M_2S_3 structure type. The initial structural model was that proposed by Jellinek[6] for rhombohedral Cr_2S_3, with unit cell parameters related to those of the primitive hexagonal NiAs unit cell by: $a \approx \sqrt{3}a_p$ and $c \approx 3c_p$. Initially, the site occupancy factors (SOF) for V and Cr at each metal site were allowed to vary, with the constraint that all metal sites remained fully occupied (i.e., SOF(Cr) + SOF(V) = 1 on every site). Subsequent removal of these constraints did not result in any changes to the SOFs of sites in the fully occupied layer. Disordering of cations in the vacancy layer would cause partial occupancy of a second 6(*c*) site, which is empty in the ideal structure. When the SOF(V) and SOF(Cr) at this site were allowed to vary freely, no deviation from zero was obtained for the material with a composition of $x = 0.33$, while a low refined SOF(Cr) resulted for the $x = 0.35$ phase. The refinements therefore demonstrate that the vacancies are confined to the partially occupied layer in which there is almost complete two-dimensional ordering. Final observed, calculated, and difference profiles for neutron and X-ray diffraction data for the composition $x = 0.33$ are shown in Figure 2. The final refined parameters for materials in this composition range are presented in Table 2.

Composition Range $0.40 \leq x \leq 0.46$. Materials in the composition range $0.40 \leq x \leq 0.46$ crystallize in the trigonal M_2S_3-type structure. The two-dimensional ordering of the vacancies within the partially occupied layer is similar to that of rhombohedral M_2S_3, but the manner in which the vacancy layers order along the stacking direction (*c* axis) differs as shown in Figure 3. In the ideal trigonal M_2S_3 structure, cations in the vacancy layer occupy only the 2(*c*) site. However, neutron diffraction investigations[8] on trigonal Cr_2S_3 have shown that the ordering of the vacancies is incomplete, each of the 2(*c*), 2(*a*), and 2(*d*) sites in the vacancy layer being partially occupied. Therefore, the initial structural model had V and Cr cations at these sites and at the 2(*b*) and 4(*f*) sites in the fully occupied layer. The SOF(V) and SOF(Cr) on every site were

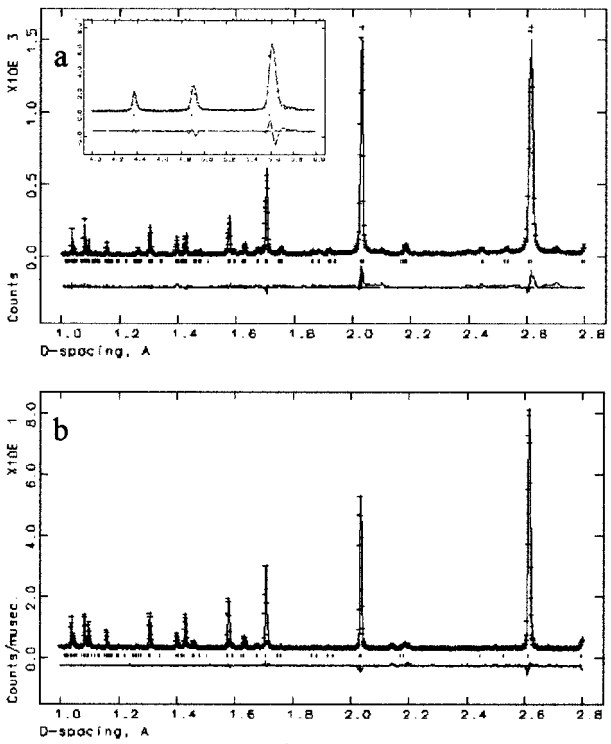

Figure 2. Observed (crosses), calculated (upper full line), and difference (lower full line) profiles for $V_{0.33}CrS_2$ at room temperature: (a) X-ray data (the inset shows reflections at longer *d* spacings, characteristic of the rhombohedral M_2S_3 structure) and (b) neutron data (reflection positions are marked).

Table 2. Final Refined Parameters for Materials with the Rhombohedral M_2S_3 Structure (Space Group $R\bar{3}$)[a]

		x in V_xCrS_2	
		0.33	0.35
	a (Å)	5.91079(5)	5.90948(5)
	c (Å)	16.7829(2)	16.7865(2)
(M(1))	SOF(V)	0.399(8)	0.49(1)
	SOF(Cr)	0.567(6)	0.526(8)
	B (Å^2)	0.42(4)	0.37(5)
(M(2))	SOF(V)	–	0
	SOF(Cr)	–	0.028(3)
	z	–	0.163(4)
	B (Å^2)	–	0.37(5)
[M(3)]	SOF(V)	0.205(9)	0.20(1)
	SOF(Cr)	0.795(9)	0.80(1)
	B (Å^2)	0.53(4)	0.62(5)
[M(4)]	SOF(V)	0.202(6)	0.222(6)
	SOF(Cr)	0.798(6)	0.778(6)
	z	0.32601(6)	0.32598(8)
	B (Å^2)	0.29(2)	0.26(3)
S(1)	x	0.3386(3)	0.3381(3)
	y	−0.0036(3)	−0.0040(3)
	z	0.25226(5)	0.25239(5)
	B (Å^2)	0.49(1)	0.49(1)
R_{wp}	X-ray	12.3%	11.6%
	neutron	1.5%	1.3%
χ^2		1.3	1.8
crystallographic composition		$(V_{0.13}Cr_{0.19})$-$[V_{0.20}Cr_{0.80}]S_2$	$(V_{0.16}Cr_{0.19})$-$[V_{0.21}Cr_{0.79}]S_2$

[a] Parentheses and square brackets denote cation sites in the vacancy and fully occupied layers respectively. (M(1)) on 3(*b*) (0,0,1/2); (M(2)) on 6(*c*) (0,0,*z*); [M(3)] on 3(*a*) (0,0,0); [M(4)] on 6(*c*) (0,0,*z*) and S(1) on 18(f) (*x*,*y*,*z*).

(25) Rice, C. E.; Robinson, W. R. *J. Solid State Chem.* **1977**, *21*, 145.

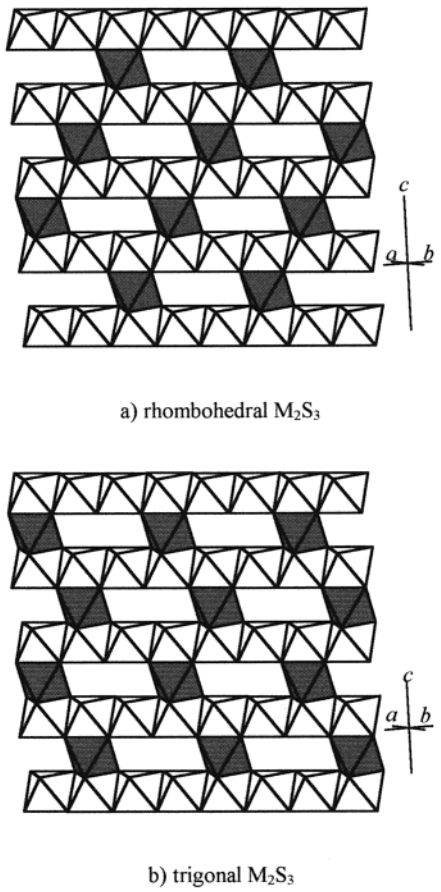

Figure 3. Sections through the (110) plane of the structures of (a) rhombohedral M_2S_3 and (b) trigonal M_2S_3, shown as packings of MS_6 octahedra. White octahedra represent MS_6 units in the fully occupied layer and gray octahedra represent MS_6 units in the partially occupied layer.

allowed to vary, with the constraint that the total SOF of sites in the fully occupied layer remained at unity. No significant changes in SOFs were observed on removal of this constraint, confirming that vacancies are confined to the partially occupied layer. Final observed, calculated, and difference profiles for neutron and X-ray diffraction data for the composition $x = 0.46$ are shown in Figure 4 and the refined parameters for materials in this composition range are given in Table 3.

Composition Range $0.53 \leq x \leq 0.76$. Materials over this composition range crystallize in the monoclinic M_3S_4 type structure with similar unit cell parameters to those of VCr_2S_4[26] (space group $I2/m$), which are related to those of NiAs by $a \approx \sqrt{3}a_p$, $b \approx a_p$, and $c \approx 2c_p$. In the ideal M_3S_4 structure, with $x = {}^1/_2$, cations in the vacancy layer occupy the 2(a) site and cations in the fully occupied layer occupy the 4(i) site.[27] Diffraction data reveal that in the V_xCrS_2 system, the M_3S_4 structure is stable over a wide composition range, $0.53 \leq x \leq 0.76$. Values of x larger than the ideal value of ${}^1/_2$, correspond either to sulfur deficiency, or to a cation-rich structure in which the normally empty 2(d) site in the vacancy layer is partially occupied. Structural models based on a sulfur-deficient material did not produce successful refinements. Therefore, a model based on a cation-rich structure was adopted, with

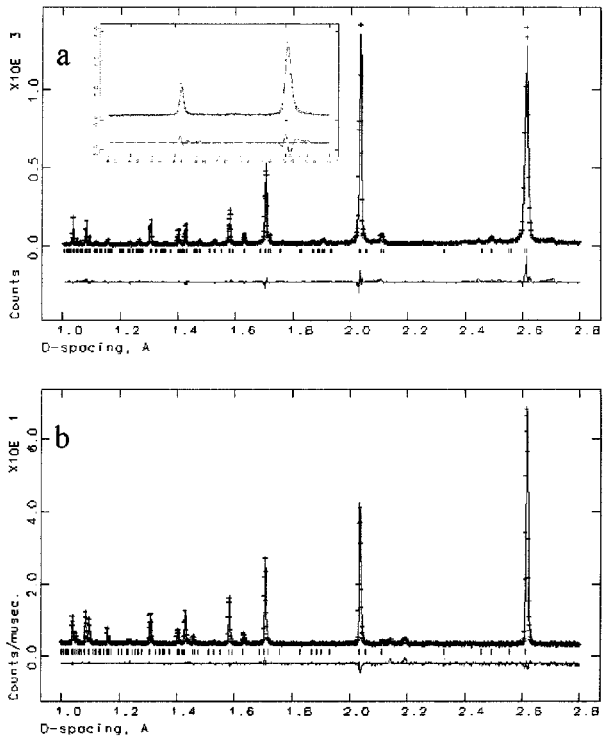

Figure 4. Observed (crosses), calculated (upper full line) and difference (lower full line) profiles for $V_{0.46}CrS_2$ at room temperature: (a) X-ray data (the inset shows reflections at longer d spacings, characteristic of the trigonal M_2S_3 structure) and (b) neutron data (reflection positions are marked).

Table 3. Final Refined Parameters for Materials with the Trigonal M_2S_3 Structure (space group $P\bar{3}1c$)[a]

		x in V_xCrS_2	
		0.40	0.46
	a (Å)	5.91133(5)	5.90800(6)
	c (Å)	11.2154(1)	11.2254(1)
(M(1))	SOF(V)	0.52(1)	0.52(2)
	SOF(Cr)	0.35(1)	0.34(1)
	B (Å^2)	0.65(5)	0.57(7)
(M(2))	SOF(V)	0.01(2)	0.04(2)
	SOF(Cr)	0.22(1)	0.21(1)
	B (Å^2)	0.65(5)	0.57(7)
(M(3))	SOF(V)	0.05(1)	–
	SOF(Cr)	0	–
	B (Å^2)	0.65(5)	–
[M(4)]	SOF(V)	0.23(1)	0.24(2)
	SOF(Cr)	0.77(1)	0.76(2)
	z	0.9896(1)	0.9896(2)
	B (Å^2)	0.41(2)	0.40(2)
[M(5)]	SOF(V)	0.20(2)	0.24(3)
	SOF(Cr)	0.80(2)	0.76(3)
	B (Å^2)	0.41(2)	0.40(2)
S(1)	x	0.3298(7)	0.330(1)
	y	−0.0067(2)	−0.0057(3)
	z	0.37850(6)	0.37835(8)
	B (Å^2)	0.51(1)	0.51(1)
R_{wp}	X-ray	11.1%	11.3%
	neutron	1.4%	1.6%
χ^2		1.3	1.0
crystallographic composition		$(V_{0.19}Cr_{0.19})$-$[V_{0.22}Cr_{0.78}]S_2$	$(V_{0.19}Cr_{0.18})$-$[V_{0.24}Cr_{0.76}]S_2$

[a] Parentheses and square brackets denote cation sites in the vacancy and fully occupied layers respectively. (M(1)) on 2(c) (${}^1/_3,{}^2/_3,{}^1/_4$); (M(2)) on 2(a) (0,0,${}^1/_4$); (M(3)) on 2(d) (${}^2/_3,{}^1/_3,{}^1/_4$); [M(4)] on 4(f) (${}^1/_3,{}^2/_3, z$); [M(5)] on 2(b)(0,0,0) and S(1) on 12(i) (x,y,z).

cations occupying the 4(i), 2(a), and 2(d) sites. The SOF(V) and SOF(Cr) at every site were allowed to vary, with the same constraint on SOFs as applied to the trigonal

(26) Powell, A. V.; Colgan, D. C. *Mater. Sci. Forum*. **1996**, *228*, 831.
(27) Okazaki, A.; Hirakawa, K. *J. Phys. Soc. Jpn*. **1956**, *11*, 930.

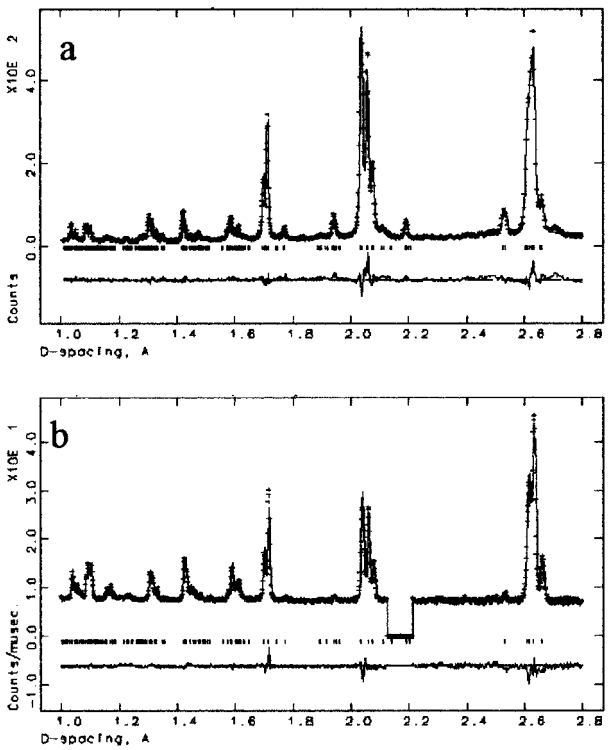

Figure 5. Observed (crosses), calculated (upper full line) and difference (lower full line) profiles for $V_{0.67}CrS_2$ at room temperature: (a) X-ray data and (b) neutron data (reflection positions are marked).

M_2S_3 refinements. Final observed, calculated, and difference profiles for neutron and X-ray diffraction data for the composition $x = 0.67$ are shown in Figure 5 and the refined parameters for materials over this composition range are given in Table 4.

Composition Range $0.76 < x < 0.90$. For products over the range $0.76 < x < 0.90$, powder X-ray diffraction data can be indexed on the basis of a hexagonal unit cell, consistent with an ordered M_7S_8 ($x = {}^3/_4$) structure, similar to that of 3C-Fe_7Se_8 reported by Parise et al.[28] Rietveld refinements were carried out in the space group $P3_121$ using, for the initial structural model, the parameters for 3C-Fe_7Se_8. The hexagonal unit cell parameters are related to those of the primitive NiAs unit cell by $a \approx 2a_p$; $c \approx 3c_p$. Initially, both V and Cr cations were introduced to each of the five metal sites and SOFs were refined with the constraint that the overall SOF at each site was unity. However at this stage, instabilities in the sulfur positional parameters would not allow the refinement to reach convergence and the goodness of fit indicator remained above 3. Therefore, following the approach of Keller-Besrest et al.,[29] an additional metal site was introduced within the vacancy layer (M(3) in Table 5). No constraints on the overall SOF of this site were applied, and constraints on the SOFs of metal sites in the vacancy layer were removed. This lead to convergence of the refinement, with a slight improvement in the goodness of fit indicator, resulting in the final observed, calculated and difference profiles, shown in Figure 6, and the refined parameters of Table 5.

Composition Range $0.90 \leq x < 0.93$. A single-phase region was found over the composition range $0.90 \leq x < 0.93$. Powder diffraction patterns for materials in this range do not exhibit any reflections corresponding to a supercell of the NiAs type, indicating the absence of two-dimensional ordering of vacancies. Vacancies may either be distributed randomly in every cation layer (interlayer disorder) or confined to every second cation layer and disordered within that layer (intralayer disorder).[30] A structure exhibiting intralayer disorder can be described in the space group $P\bar{3}ml$ whereas interlayer disorder corresponds to the space group $P6_3/mmc$. In the latter, $(00l)$ reflections with $l = 2n + 1$ are prohibited. The absence of these characteristic $(00l)$ reflections resulted in the refinements being carried out in the space group $P6_3/mmc$, using the structure of hexagonal VS[31] for the initial structural model. Final observed, calculated, and difference profiles for neutron and X-ray diffraction data for the composition $x = 0.90$ are shown in Figure 7 and the refined parameters are given in Table 6.

Transport Properties. Conductivity measurements were carried out for selected single-phase materials in the V_xCrS_2 series. As shown in Figure 8, plots of resistivity (ρ) vs temperature (T) exhibit negative slopes, consistent with semiconducting behavior. The magnitude of $|d\rho/dT|$ decreases with increasing vanadium content, which may indicate that with increasing x, a semiconductor−metal boundary is approached. In all cases, the temperature dependence of the resistivity does not follow an Arrhenius law. However, plots of $\ln(\rho)$ vs $T^{-1/4}$ are linear over a wide temperature range, consistent with a variable range hopping conduction mechanism.[32] At low values of x, a kink can be observed in the $\rho(T)$ curves at $T \approx 90$ K, as illustrated by the inset to Figure 8. This feature becomes weaker with increasing vanadium content, and disappears at $x > 0.46$. A similar anomaly in the electrical resistivity has been observed at the Curie temperature in rhombohedral Cr_2S_3.[9]

Magnetic Properties. Magnetic susceptibility measurements were carried out for a representative composition in each single-phase region. The temperature dependence of the magnetic susceptibility of these materials is plotted in Figure 9. The magnetic properties show a much greater dependence on composition than do the transport properties. The magnetic susceptibility of $V_{0.33}CrS_2$ (rhombohedral M_2S_3 structure) shows a large increase in the spontaneous magnetization at lower temperatures, which is attributed to the onset of long-range magnetic order. The ordering temperature (T_C) was determined as 100(10) K. Above 175 K, data follow a Curie−Weiss law with an effective magnetic moment of 2.97(4) μ_B (Table 7). The negative curvature of the plot of $1/\chi$ vs T below $\sim 2T_C$ is characteristic of ferrimagnetic materials.[33] The magnetization was measured as a function of field at 10 K and the ferrimagnetic moment, obtained by extrapolation of the linear portion of $M(H)$ to zero-field, determined as 0.369(2) μ_B per

(28) Parise, J. B.; Nakano, A.; Tokonami, M.; Morimoto, N. *Acta Crystallogr. B* **1979**, *35*, 1210.
(29) Keller-Besrest, F.; Collin, G.; Comès, R. *Acta Crystallogr. B* **1982**, *38*, 296.
(30) Kosuge, K. *Chemistry of Non-Stoichiometric Compounds*; Oxford University Press: Oxford, 1993.
(31) Biltz, W.; Koecher, A. *Z. Anorg. Allg. Chem.* **1939**, *241*, 324.
(32) Mott, N. F.; Davis, E. A. *Electronic Processes in Non-Crystalline Materials*, 2nd ed.; Oxford University Press: Oxford, 1979.
(33) Crangle, J. *The Magnetic Properties of Solids*; Edward Arnold: London, 1977.

Table 4. Final Refined Parameters for Materials with the Monoclinic M_3S_4 Structure (space group *I2/m*)

		x in V_xCrS_2					
		0.53	0.58	0.63	0.67	0.70	0.76
	a (Å)	5.9449(2)	5.9461(2)	5.9536(2)	5.9574(2)	5.9562(1)	5.9511(1)
	b (Å)	3.3834(1)	3.3773(1)	3.3942(1)	3.4009(1)	3.40467(8)	3.41630(9)
	c (Å)	11.2263(4)	11.2353(4)	11.3310(4)	11.3825(4)	11.4120(3)	11.4716(3)
	β (deg)	91.573(2)	91.680(2)	91.310(2)	91.127(2)	90.995(1)	90.620(1)
(M(1))	SOF(V)	0.477(7)	0.497(7)	0.485(7)	0.449(8)	0.475(7)	0.471(9)
	SOF(Cr)	0.523(7)	0.503(7)	0.515(7)	0.551(8)	0.525(7)	0.529(9)
	B (Å^2)	0.35(6)	0.23(5)	0.57(5)	0.77(5)	0.74(5)	0.83(4)
(M(2))	SOF(V)	−	0.007(8)	0.027(8)	0.068(9)	0.092(9)	0.14(1)
	SOF(Cr)	−	0.031(5)	0.111(6)	0.149(7)	0.187(6)	0.269(8)
	B (Å^2)	−	0.23(5)	0.57(5)	0.77(5)	0.74(5)	0.83(4)
[M(3)]	SOF(V)	0.285(6)	0.326(5)	0.350(4)	0.369(5)	0.388(4)	0.430(4)
	SOF(Cr)	0.715(6)	0.674(5)	0.650(4)	0.631(5)	0.612(4)	0.570(4)
	x	−0.0225(3)	−0.0231(3)	−0.0176(3)	−0.0169(4)	−0.0153(4)	−0.0137(5)
	z	0.2583(2)	0.2581(2)	0.2579(2)	0.2571(2)	0.2568(2)	0.2550(3)
	B (Å^2)	0.56(3)	0.55(3)	0.66(3)	0.57(4)	0.65(3)	0.81(5)
S(1)	x	0.3399(3)	0.3383(3)	0.3383(3)	0.3368(3)	0.3363(3)	0.3364(4)
	z	0.3648(2)	0.3645(1)	0.3657(1)	0.3663(1)	0.3665(1)	0.3678(2)
	B (Å^2)	0.24(2)	0.26(2)	0.41(2)	0.34(2)	0.35(2)	0.41(2)
S(2)	x	0.3331(3)	0.3343(3)	0.3339(3)	0.3340(3)	0.3339(3)	0.3328(4)
	z	0.8818(2)	0.8831(1)	0.8809(1)	0.8804(1)	0.8803(1)	0.8786(2)
	B (Å^2)	0.46(3)	0.40(2)	0.46(2)	0.48(2)	0.49(2)	0.54(2)
R_{wp}	X-ray	10.3%	10.9%	10.3%	9.3%	10.2%	10.1%
	neutron	1.6%	1.6%	1.3%	1.4%	1.4%	1.2%
χ^2		1.0	1.4	1.2	1.0	1.0	1.1
crystallographic composition		$(V_{0.24}Cr_{0.26})$-$[V_{0.28}Cr_{0.72}]S_2$	$(V_{0.25}Cr_{0.27})$-$[V_{0.33}Cr_{0.67}]S_2$	$(V_{0.26}Cr_{0.31})$-$[V_{0.35}Cr_{0.65}]S_2$	$(V_{0.26}Cr_{0.35})$-$[V_{0.37}Cr_{0.63}]S_2$	$(V_{0.28}Cr_{0.36})$-$[V_{0.39}Cr_{0.61}]S_2$	$(V_{0.31}Cr_{0.40})$-$[V_{0.43}Cr_{0.57}]S_2$

[a] Parentheses and square brackets denote cation sites in the vacancy and fully occupied layers respectively. (M(1)) on 2(*a*) (0,0,0); (M(2)) on 2(*d*) ($^1/_2$,$^1/_2$,0); [M(3)], S(1) and S(2) on 4(*i*) (*x*,0,*z*).

Table 5. Final Refined Parameters for the Material $V_{0.80}CrS_2$, with the Trigonal 3C-M_7S_8 Structure (space group $P3_121$)[a]

atom	site	x	y	z	B (Å^2)	SOF
(M(1))	6(*c*)	0.513(2)	0.496(3)	0.3308(4)	0.55(2)	V 0.49(2)
						Cr 0.51(2)
(M(2))	3(*a*)	0.019(4)	0.0	$^1/_3$	0.55(2)	V 0.18(4)
						Cr 0.48(3)
(M(3))	3(*a*)	0.492(7)	0.0	$^1/_3$	0.55(2)	V 0.0
						Cr 0.18(2)
[M(4)]	6(*c*)	0.479(2)	0.486(2)	0.1605(4)	0.55(2)	V 0.51(1)
						Cr 0.49(1)
[M(5)]	3(*b*)	0.015(3)	0.0	$^5/_6$	0.55(2)	V 0.41(2)
						Cr 0.59(2)
[M(6)]	3(*b*)	0.487(2)	0.0	$^5/_6$	0.55(2)	V 0.43(2)
						Cr 0.57(2)
S(1)	6(*c*)	0.166(1)	0.334(1)	0.0756(2)	0.42(1)	1.0
S(2)	6(*c*)	0.336(2)	0.167(2)	0.2482(3)	0.42(1)	1.0
S(3)	6(*c*)	0.664(2)	0.328(1)	0.0866(3)	0.42(1)	1.0
S(4)	6(*c*)	0.159(1)	0.827(2)	0.0884(2)	0.42(1)	1.0

crystallographic composition: $(V_{0.29}Cr_{0.42})[V_{0.47}Cr_{0.54}]S_2$

[a] Parentheses and square brackets denote cation sites in the vacancy and fully occupied layers respectively. a = 6.85625(3); c = 17.2504(2) Å. X-ray: R_{wp} = 12.5%. Neutron: R_{wp} = 1.2%. χ^2 = 2.84.

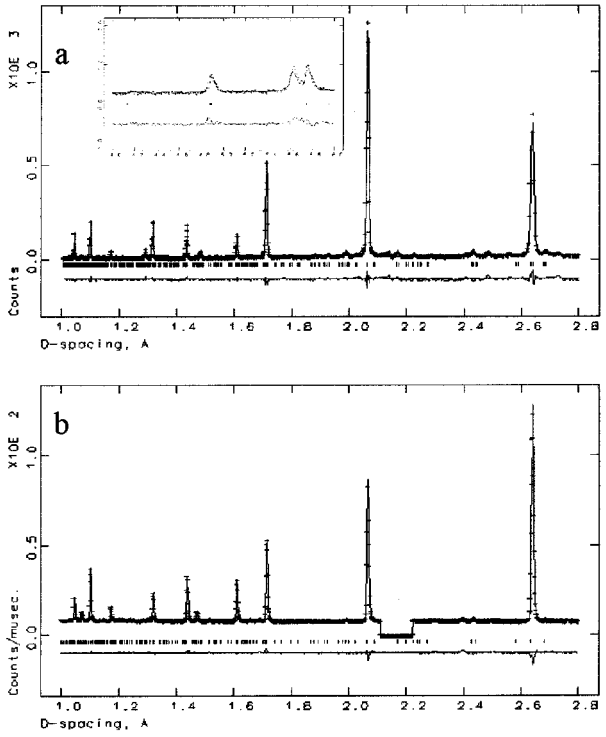

Figure 6. Observed (crosses), calculated (upper full line), and difference (lower full line) profiles for $V_{0.80}CrS_2$ at room temperature: (a) X-ray data (the inset shows reflections at longer d spacings, characteristic of the 3C-M_7S_8 structure) and (b) neutron data (reflection positions are marked).

metal atom. The magnetic susceptibility data of $V_{0.46}CrS_2$ (trigonal M_2S_3 structure) above 160 K, follow a Curie−Weiss law, with an effective magnetic moment of 2.84(2) μ_B. At lower temperatures, both zfc and fc data show a marked increase. The zfc susceptibility passes through a maximum at 35 K below which the fc susceptibility shows a slight increase, suggesting the presence of some residual spontaneous magnetization at low temperatures. The behavior of the zfc susceptibility is similar to that of trigonal Cr_2S_3, which exhibits a spiral magnetic structure at low temperatures.[8] The magnetic susceptibility of $V_{0.63}CrS_2$ (monoclinic M_3S_4 structure) shows a considerably weaker temperature dependence than is observed at lower vanadium contents. The zfc susceptibility has a broad maximum at ~40 K. The zfc and fc data overlie each other at higher temperatures but begin to diverge on cooling toward this maximum. Data for the isostructural $V_yCr_{3-y}S_4$ phases, which show a similar behavior, have been interpreted in terms of a spin-glass transition,[21,34] the transition temperature increasing with decreasing vanadium con-

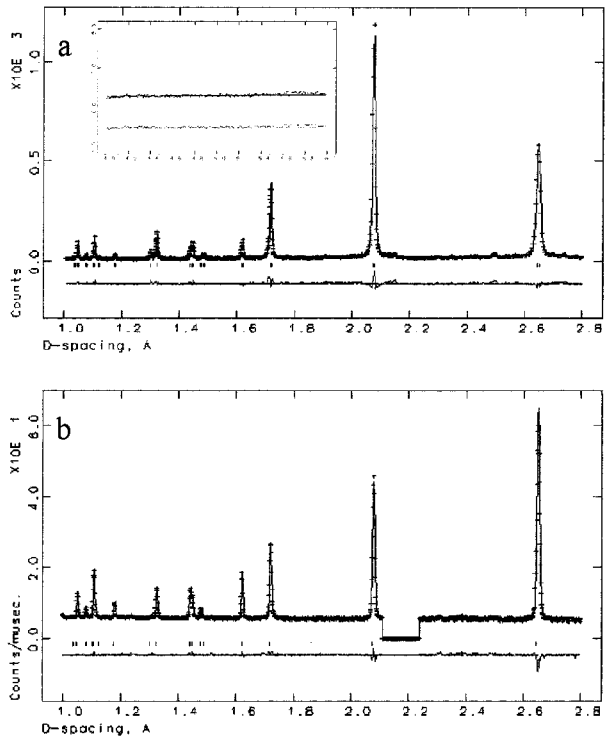

Figure 7. Observed (crosses), calculated (upper full line), and difference (lower full line) profiles for $V_{0.90}CrS_2$ at room temperature: (a) X-ray data (the inset shows the absence of (00*l*) reflections at longer *d* spacings) and (b) neutron data (reflection positions are marked).

Table 6. Final Refined Parameters for the Material $V_{0.90}CrS_2$ (Space Group $P6_3/mmc$)[a]

atom	site	x	y	z	B (Å^2)	SOF
M(1)	2(*a*)	0	0	0.5	0.99(2)	V 0.406(5) Cr 0.484(3)
S	2(*c*)	$^1/_3$	$^2/_3$	$^1/_4$	0.60(1)	1.0
crystallographic composition: $V_{0.81}Cr_{0.97}S_2$						

[a] $a = 3.43854(5)$; $c = 5.7966(1)$ Å. X-ray: $R_{wp} = 10.6\%$. Neutron: $R_{wp} = 1.4\%$. $\chi^2 = 1.2$.

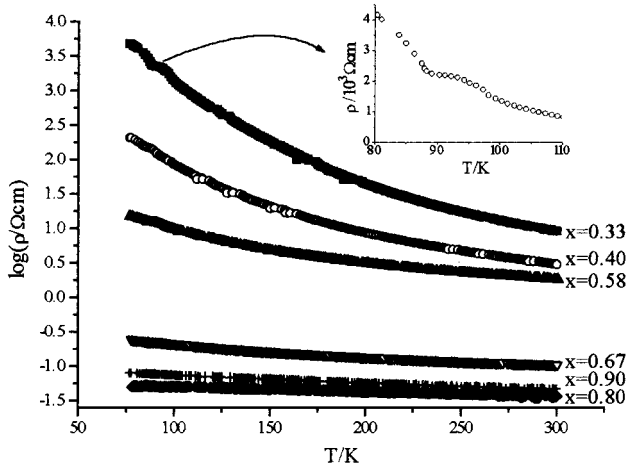

Figure 8. Temperature dependence of the electrical resistivity for representative single-phase compositions in the series V_xCrS_2. The inset shows the kink at the Curie temperature for the composition $V_{0.33}CrS_2$.

tent. In common with these phases, magnetic susceptibility data for $V_{0.63}CrS_2$ over the temperature range $50 \le T/K \le 300$ are well described by a modified Curie–Weiss law ($\chi = \chi_0 + C/(T - \theta)$), where χ_0 is a temperature-independent paramagnetic term (Table 7). The magnetic susceptibility data for $V_{0.80}CrS_2$ above 170 K follow a Curie–Weiss law, with an effective magnetic moment of 2.72(3) μB. The susceptibility maximum at 150(10) K, similar to that observed in Cr_7S_8 at 125 K, suggests that this material orders antiferromagnetically at this temperature. The divergence of fc and zfc data at lower temperatures is a sign of the existence of some degree of magnetic frustration. The magnetic susceptibility data for $V_{0.90}CrS_2$ show an even weaker temperature dependence but suggest that the onset of long-range magnetic order is at 230(10) K.

Discussion

Five single-phase regions have been identified in the V_xCrS_2 system. These regions are generally narrow, with the exception of that of the M_3S_4 structure, which extends over the composition range $0.53 \le x \le 0.76$. The extended homogeneity range of this structure means that the M_5S_6 structure, observed in the Cr_xCrS_2 series at $x = 0.7$,[6] is absent from the ternary series described here. Although stoichiometry ranges in the Cr_xCrS_2 system are very narrow at low temperatures, studies carried out at 700 °C determined rather wide phase ranges for Cr_3S_4 and Cr_7S_8.[35] The analogous selenides Cr_xCrSe_2[36] and the sulfides V_xVS_2[15] and Fe_xVS_2[37] show similarly wide homogeneity ranges for the M_3S_4 phase.

It was not possible to obtain a single-phase material with a vanadium content lower than $x = 0.30$. Similar behavior has been reported for Cr_xCrS_2 under comparable synthesis conditions.[6] However, an ordered NiAs-type chromium sulfide with stoichiometry Cr_5S_8 ($x = 0.25$) can be prepared at high pressure,[38] and the same ordering scheme is observed in V_5S_8, prepared at ambient pressure.[15] Partial substitution of Cr with V in V_xCrS_2 does not seem to stabilize the M_5S_8 structure at ambient pressure.

In all single-phase materials in the V_xCrS_2 system with $x < 0.9$, there is long-range ordering of vacancies within the partially occupied layer. Although the two-dimensional superstructures of rhombohedral and trigonal M_2S_3 phases are identical, only in the former is the ordering almost complete. In the M_3S_4 structure, complete ordering of the vacancies is found when the nominal composition is close to $x = 0.5$. At higher vanadium contents, the empty octahedral site within the vacancy layer accommodates the excess cations. Vacancy ordering is also incomplete in the 3C-M_7S_8 structure observed for $V_{0.8}CrS_2$. It has been suggested that intergrowth of 3C and 4C stacking sequences may be responsible for the apparent partial two-dimensional disorder in 3C-Fe_7S_8.[29] No defect ordering was observed for $V_{0.9}CrS_2$.

The lattice parameters and the unit-cell volume per formula unit, as a function of composition, are shown in Figure 10. The volume (and c_p) is nearly constant for $x < 0.6$, but increases in a linear fashion above this

(34) Tazuke, Y. *J. Phys. Soc. Jpn.* **1986**, *55*, 2008.
(35) Young, D. J.; Smeltzer, W. W.; Kirkaldy, J. S. *J. Electrochem. Soc.* **1973**, *120*, 1221.
(36) Ohtani, T.; Fujimoto, R.; Yoshinaga, H.; Nakahira, M.; Ueda, Y. *J. Solid State Chem.* **1983**, *48*, 161.
(37) Oka, Y.; Kosuge, K.; Kachi, S. *Mater. Res. Bull.* **1980**, *15*, 521.
(38) Sleight, A. W.; Bither, T. A. *Inorg. Chem.* **1969**, *8*, 566.

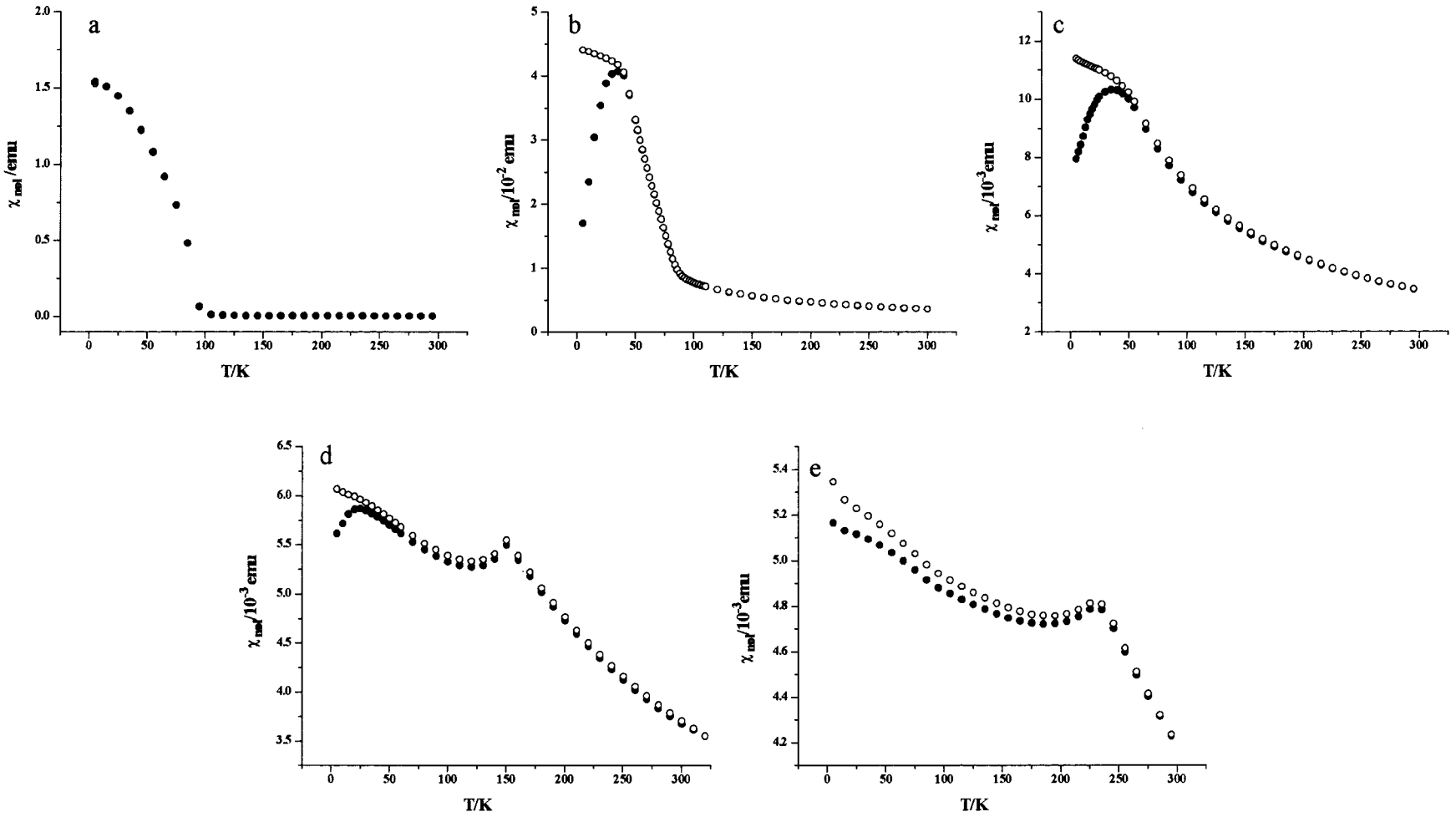

Figure 9. Zero-field cooled (solid circles) and field cooled (open circles) molar magnetic susceptibilities for the compositions: (a) $V_{0.33}CrS_2$; (b) $V_{0.46}CrS_2$; (c) $V_{0.63}CrS_2$; (d) $V_{0.80}CrS_2$; and (e) $V_{0.90}CrS_2$.

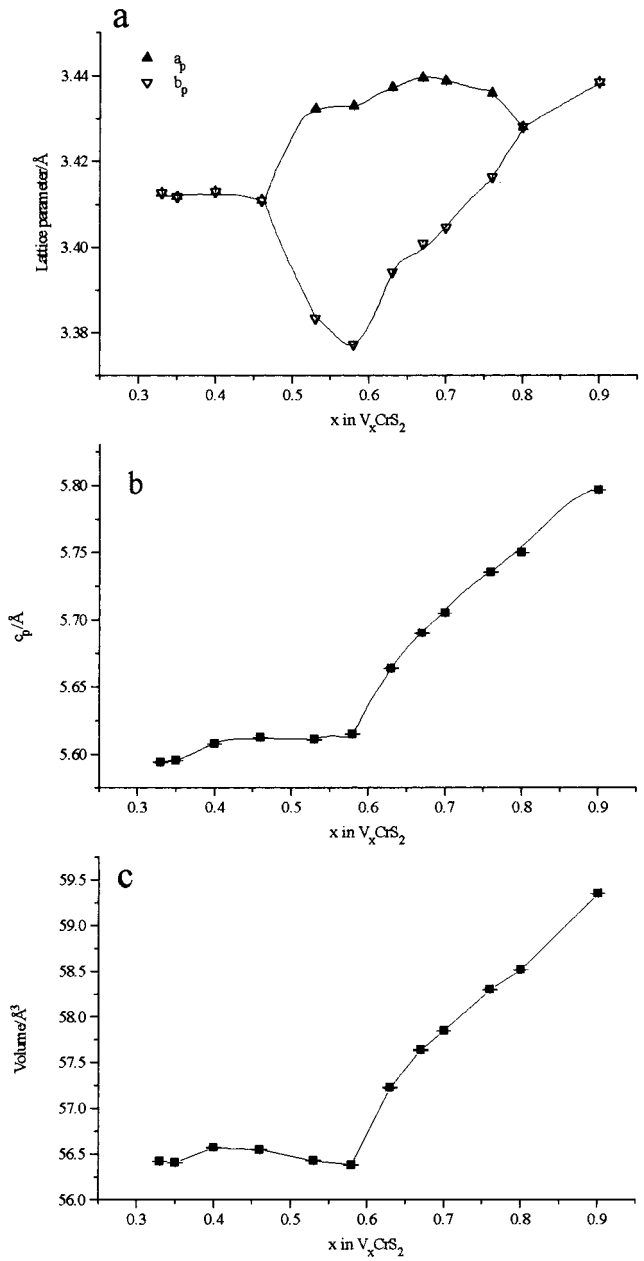

Figure 10. Composition dependence of (a) the *a* and *b* unit cell parameters; (b) the *c* unit cell parameter; and (c) the unit cell volume per formula unit. To aid comparison, lattice parameters are referred to the hexagonal NiAs unit cell. Lines are a guide to the eye.

Table 7. Magnetic Properties of Representative Single-Phase Materials in the V_xCrS_2 Series Obtained from Fits to a Curie−Weiss Expression

material	temp range (K)	C (emu K mol^{-1})	θ (K)	χ_0 (emu mol^{-1})	μ_{eff}/μ_B
$V_{0.33}CrS_2$	175−300	1.47(2)	−98(4)		2.97(4)
$V_{0.46}CrS_2$	160−300	1.47(1)	−114(3)		2.84(2)
$V_{0.63}CrS_2$	50−300	0.907(9)	−46(1)	$8.1(2) \times 10^{-4}$	2.11(2)
$V_{0.80}CrS_2$	170−300	1.67(2)	−154(4)		2.72(3)
$V_{0.90}CrS_2$	240−300	2.11(1)	−203(2)		2.97(1)

value. For all studied compositions, ∼56% of the vanadium present resides in sites in the fully occupied layer, as denoted by the formalism $(V_{0.44x}Cr_{0.56x})[V_{0.56x}Cr_{1-0.56x}]S_2$, where parentheses and square brackets represent sites in the partially and fully occupied layers, respectively. Every cation in the fully occupied layer has six nearest neighbor cations within the layer. In the rhombohedral M_2S_3, trigonal M_2S_3 and M_7S_8 phases, all six cation−cation distances are similar, and the metal atoms form a regular hexagonal array. However, in the M_3S_4 phase this array is distorted, resulting in the formation of zigzag chains parallel to the *b* axis. This type of distortion has previously been observed in materials with the M_3S_4 structure type.[39,40] The zigzag chains may favor metallic behavior, as the result of direct $t_{2g}-t_{2g}$ overlap, providing the cation−cation separation is below a critical value R_C.[41] The semiconducting behavior of the V_xCrS_2 materials indicates that the intrachain cation−cation separations (3.2−3.3 Å) are greater than R_C.

The metallic properties of Cr_3S_4 have been attributed to the presence of a partially filled band, arising from covalent mixing of cation e_g states and antibonding anion p states.[12] Band structure calculations reveal a similar interaction in hexagonal CrS (high temperature form)[42] and rhombohedral Cr_2S_3.[43] Furthermore, the introduction of vacancies to the cation sublattice, in going from CrS (NiAs structure) to Cr_2S_3 (ordered defect structure), leaves the overall form of the nonmagnetic density of states unchanged. Therefore, a partially filled e_g band results in metallic behavior for Cr_3S_4, Cr_5S_6, Cr_7S_8, and hexagonal CrS. Stoichiometric Cr_2S_3 contains only Cr^{3+}:d^3; the e_g band is hence empty and the material is semiconducting.

The substitution of chromium by vanadium on going from Cr_xCrS_2 to V_xCrS_2 reduces the degree of covalent bonding between the cation-d and anion-p states; decreases the formal electron count; and introduces substitutional disorder at the cation sites in both layers. For V_xCrS_2 with $x < 0.5$, the e_g band is empty and the t_{2g} levels are partially occupied. The latter are effectively localized, as the cation−cation distances within the fully occupied layer are considerably greater than R_C, resulting in semiconducting behavior. The rigid band model also predicts semiconducting behavior for $x = 0.5$[12] but metallic behavior at higher *x* values as e_g levels are occupied. However, since all single-phase materials in the V_xCrS_2 system are semiconductors, it appears that the effects of substitutional disorder are significant. This introduces a random potential which reduces the mean free path of the electrons.[44]

In V_xCrS_2 materials with $x < 0.46$, there is an anomaly in the $\rho(T)$ curves around the magnetic ordering temperature. Similar behavior has been observed in rhombohedral n-type Cr_2S_3 at the Curie temperature.[8] It has been explained in terms of an exchange interaction between the spins of the charge carriers and the localized magnetic moments, which leads to spin splitting of the conduction band and spin−disorder scattering of the charge carriers. Similar anomalies

(39) Powell, A. V.; Colgan, D. C.; Vaqueiro, P. *J. Mater. Chem.* **1999**, *9*, 485.
(40) Bouchard, R. B.; Robinson, W. T.; Wold, A. *Inorg. Chem.* **1966**, *5*, 977.
(41) Goodenough, J. B. *Magnetism and the Chemical Bond*; Wiley: New York, 1963.
(42) Dijkstra, J.; van Bruggen, C. F.; Haas, C.; de Groot, R. A. *J. Phys.: Condens. Matter.* **1989**, *1*, 9163.
(43) Raybaud, P.; Hafner, J.; Kresse, G.; Toulhoat, H. *J. Phys.: Condens. Mater.* **1997**, *9*, 11107.
(44) Mott, N. F. *Metal−Insulator Transitions*; Taylor and Francis; 1990.

have been observed in other magnetic semiconductors, such as $FeCr_2S_4$.[45] Further studies would be required to clarify the origin of this behavior in the V_xCrS_2 materials.

All materials exhibit Curie−Weiss behavior at higher temperatures, although there is a significant temperature independent contribution to the magnetic susceptibility of the M_3S_4 type phases. The theoretical Curie constant for $V_{0.33}CrS_2$ is 2.21 emu K mol^{-1}. If a localized electron picture is valid, the Curie constant would increase with increasing vanadium content, reaching a limiting value of 4.89 emu K mol^{-1} at the hypothetical composition $VCrS_2$, assuming divalent Cr and V. However, examination of Table 7 reveals that the Curie constant of $V_{0.33}CrS_2$ is somewhat lower than the theoretical value and shows relatively little dependence on vanadium content; the reduction in the case of $V_{0.63}CrS_2$ resulting from the introduction of a temperature independent paramagnetic term. These observations indicate that a localized electron picture is inapplicable to these materials and that the electrons are more likely to reside in narrow bands.[46,47] The effective magnetic moment is then a measure of the imbalance in the populations of the different spin-states. Examination of the plots of susceptibility vs temperature suggests that with the exception of $V_{0.63}CrS_2$, long-range magnetic order is established for all phases. Negative Weiss constants indicate that the dominant exchange interactions are antiferromagnetic. While $V_{0.9}CrS_2$ and $V_{0.8}CrS_2$ appear to order antiferromagnetically, the behavior of $V_{0.33}CrS_2$ and $V_{0.46}CrS_2$ is more complex. Both show a large increase in susceptibility at low temperature, indicating a spontaneous magnetization in the magnetic ground state. Rhombohedral Cr_2S_3 shows similar behavior below 120 K. The magnetic structure of this material, determined by powder neutron diffraction,[48,49] comprises three magnetic sublattices. As these couple to produce a zero net magnetization, it has been suggested[50] that the observed susceptibility is the result of spin-canting. In the isostructural ternary phase V_xCrS_2 ($0.30 < x \leq 0.35$), the variation in the V:Cr ratio at the sites on each sublattice could lead to a spontaneous moment without spin-canting. Susceptibility data for the materials V_xCrS_2 with the trigonal M_2S_3 structure ($0.40 \leq x \leq 0.46$), are similar to those of the isostructural binary phase, which has a complex magnetic structure with a spiral spin configuration.[8] It is not possible to determine from the susceptibility data alone, whether the partial replacement of chromium in Cr_2S_3 by vanadium disrupts the magnetic exchange pathways. A low-temperature neutron diffraction study would be required to confirm the existence of magnetic ordering.

Acknowledgment. We thank EPSRC for a grant in support of our neutron scattering program, The Leverhulme Trust for a research fellowship for P.V. and Dr. R. I. Smith (Rutherford Appleton Laboratory) for assistance with the collection of neutron diffraction data. Dr. M. P. Crosnier-Lopez (Université du Maine) is thanked for the electron microscopy study.

Supporting Information Available: Tables of bond lengths and bond angles. This material is available free of charge via the Internet at http://pubs.acs.org.

CM000265C

(45) Bouchard, R. J.; Russo, P. A.; Wold, A. *Inorg. Chem.* **1965**, *4*, 685.
(46) Wilson, J. A. *Adv. Phys.* **1972**, *21*, 143.
(47) Cyrot, M. *Philos. Mag.* **1972**, *25*, 1031.
(48) Bertaut, E. F.; Cohen, J.; Lambert-Andron, B.; Mollard, P. *J. Physique* **1968**, *29*, 813.
(49) Popma, T. J. A.; Haas, C.; van Laar, B. *J. Phys. Chem. Solids* **1971**, *32*, 581.
(50) Sugiura, T.; Iwahashi, K.; Horai, K.; Masuda, Y. *J. Phys. Soc. Jpn.* **1975**, *38*, 365.